Available online at www.sciencedirect.com
ScienceDirect
Bioorganic & Medicinal Chemistry 16 (2008) 5778–5787
Bioorganic & Medicinal Chemistry

Thermodynamics and fluorescence studies of the interactions of cyclooctapeptides with Hg^{2+}, Pb^{2+}, and Cd^{2+}

Maria Ngu-Schwemlein,* Willie Gilbert, Kshawna Askew and Stefanie Schwemlein

Department of Chemistry, Winston-Salem State University, 601 M.L. King, Jr. Drive, W.B. Atkinson Science Building, Winston-Salem, NC 27110, USA

Received 25 January 2008; revised 20 March 2008; accepted 24 March 2008
Available online 27 March 2008

Abstract—The purpose of this work is to characterize the interactions of cyclooctapeptides (**CP**) containing glutamyl and/or cysteinyl residues with common heavy-metal ions in order to facilitate the design of cyclopeptides as sensors for metal ions. Isothermal titration calorimetry studies show that cyclooctapeptides containing glutamyl and/or cysteinyl residues bind these Hg^{2+} and Pb^{2+} over Cd^{2+} and other common metal ions. Differential binding isotherms, in their interactions with Hg^{2+}, support a two-binding site model, whereas pertinent interactions with Pb^{2+} support a 2:1 stoichiometry, suggesting a **CP**/Pb^{2+}/**CP** mode of complexation. The cyclooctapeptide containing both glutamyl and cysteinyl residues shows a significant binding affinity for Hg^{2+} ($K_a = 7.6 \times 10^7\ M^{-1}$), which is both enthalpically and entropically driven. The fluorescence of these cyclooctapeptides showed pronounced fluorescence quenching responses to Hg^{2+} over Pd^{2+} and Cd^{2+}. Stern–Volmer analyses of the dependence of fluorescence intensity on Hg^{2+} and Pb^{2+} are reported. The observed trends are useful for the design of Hg^{2+} sensors based on fluorophore-tagged cyclooctapeptides.
Published by Elsevier Ltd.

1. Introduction

Optical sensors for the detection of toxic metal ions such as Hg^{2+}, Pb^{2+}, and Cd^{2+} have significant applications in environmental chemistry and biomedical research,[1–3] encompassing areas of medical and biochemical analyses and the monitoring of these toxic ions in the environment. While various types of chemical sensors for these hazardous metal ions have been reported, many of them have one or more limitations, which include low sensitivity, poor specificity, slow response, and short shelf life. Hence, the design and development of a more accurate and rapid identification of these harmful metal ions is both desirable and worthwhile. In recent years, various types of chemical sensors for toxic metal ions have been reported, ranging from small molecule fluorescent chemosensors[4–10] to macrocycles,[11–18] such as the synthetic crown ethers, azacrowns, calixerenes, and thiacyclams.[11,13] We are especially interested in developing cyclopeptide-based motifs for selective metal-ion binding and sensing.[19,20] As previously reported, cyclopeptides offer various chemical and structural features that are favorable for metal-ion chelation and sensing.[19] Specifically, fluorophore-tagged peptide macrocycles are structurally attractive. They form complexes that are generally thermodynamically and kinetically more stable than their acyclic analogs. The peptide macrocyclic framework can be readily tailored for selective interaction with certain metal ions according to their size. Cyclopeptides can also adopt stable tertiary structures to enable strategic positioning of metal coordinating groups to accommodate the coordination positions of the metal-ion concerned. Appropriate positioning of selected types of fluorophores in the cyclopeptide structural scaffold allows for a rapid, convenient, and highly sensitive signaling of the peptide–metal-ion interaction event. Additionally, the size of the cyclic peptide framework, the type (α, β, γ, and N-alkylated) and stereochemistry of the amino acid residues can be readily altered to tailor complexation of the metal-ion in different environments of interest. The chemical stability of the peptide backbone toward endopeptidases can also be readily improved by employing amino acid building blocks with alternating L- and D-stereochemistry. Moreover, the ease in chemical modification of the peptide backbone or side chain residues offers a variety of arrangements for the metal coordinating atoms (donor atoms), both in the peptide backbone and in the side chains of the cyclopeptide.

Keywords: Fluorogenic cyclopeptide; Metal-ion binding; Isothermal titration calorimetry; Fluorescence quenching; Stern–Volmer plots.
* Corresponding author. Tel.: +1 336 750 2919; fax: +1 336 750 2549; e-mail: Schwemleinmn@wssu.edu

0968-0896/$ - see front matter Published by Elsevier Ltd.
doi:10.1016/j.bmc.2008.03.058

The previous studies by our group have shown that a model amphiphatic cyclooctapeptide, containing alternating L- and D-amino acid residues, carboxylate functions and an intrinsic fluorophore (Trp), cyclo[D-Glu-Glu-D-Glu-Glu-D-Leu-Leu-D-Leu-Trp] (**CP1**) (Fig. 1), exhibited selective binding and specific fluorescent responses toward some divalent transition metal ions ($Hg^{2+} > Pb^{2+} > Zn^{2+} > Cu^{2+}$, Cd^{2+}) among the surveyed alkali (Li^+, Na^+, K^+, Cs^+), alkaline earth (Mg^{2+}, Ca^{2+}, Ba^{2+}), transition (Cu^{2+}, Zn^{2+}) and heavy-metal ions (Cd^{2+}, Pb^{2+}, Hg^{2+}).[19] In continuation of our work in exploring the cyclopeptide-based motifs for selective metal-ion binding and sensing, the present study was undertaken to develop a better understanding of the interactions of these cyclopeptides with some common toxic heavy-metal ions such as Hg^{2+}, Pb^{2+}, and Cd^{2+} by alternating the glutamyl residues with hydrophobic residues and substituting two glutamyl residues with Cys, while retaining Trp as the intrinsic fluorogenic signal. Cyclo[Glu-D-Leu-Glu-D-Leu-Glu-D-Leu-Glu-D-Trp] (**CP2**) and cyclo[Glu-D-Leu-Cys-D-Leu-Glu-D-Leu-Cys-D-Trp] (**CP3**) were prepared for this study. The metal-ion binding sites bearing carboxylate groups from glutamyl residues are clustered on one side of the cyclopeptide ring in **CP1**. We anticipated that their interactions with metal ions could be optimized by spacing them throughout the macrocycle by alternation with the hydrophobic Leu residue as depicted in **CP2**. It has long been acknowledged that selectivity for complex formation with metal ions depends on many factors, including the nature of the donor atom that invokes ligand and metal-ion chelation.[21–23] As summarized in the 'Hard and Soft Acid and Base' ideas of Pearson, the 'soft bases' effectively complex with 'soft acids' such as the heavy metal ions.[24] Accordingly, sulfur-containing calixarenes have been shown to exhibit significantly improved molecular recognition for Hg^{2+}.[25,26] Thus, **CP3** is designed to include the soft base atom S by substituting two glutamyl residues (containing metal-ion coordinating carboxylate functionalities in which the donor oxygen atom is classified as a 'hard base') with cysteinyl residues (containing the thiolate

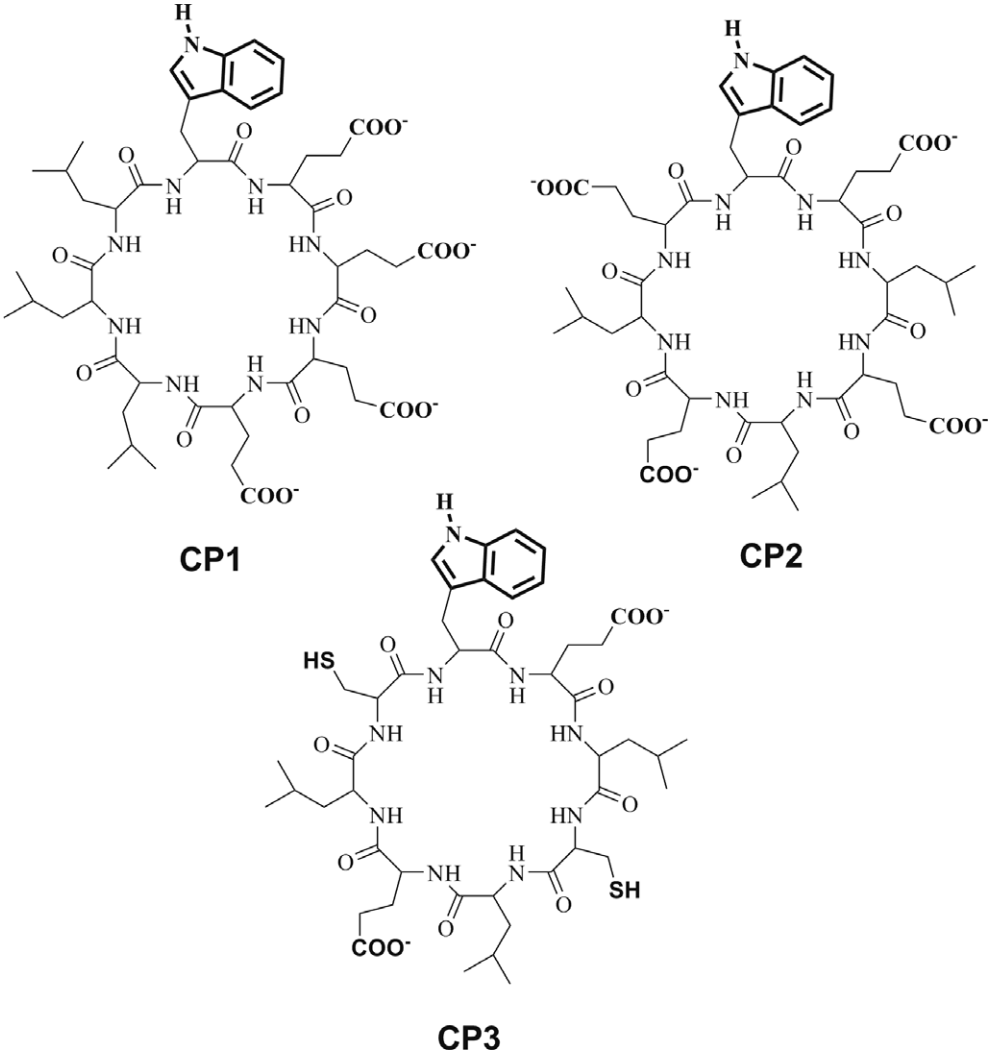

Figure 1. The chemical structures of **CP1**, **CP2**, and **CP3**: **CP1** contains 4 Glu carboxylate groups spaced adjacent to one another, imparting amphipathic in the cyclooctapeptide, **CP2** contains 4 Glu carboxylate groups spaced further apart by alternating Glu residues with hydrophobic Leu residues, and **CP3** contains 2 Glu carboxylate and 2 Cys thiolate groups spaced further apart by alternating Leu residues. The side chain coordinating atoms and the intrinsic fluorophore Trp are shown in bold.

coordinating groups where the metal-ion coordinating sulfur atom is a 'soft base') to enhance the metal-ion binding properties of these acidic cyclopeptides for Hg^{2+}.

We report here the thermodynamic parameters, enthalpy (ΔH), entropy (ΔS), and free energy (ΔG), including the binding constant (K_a), for the interactions between these cyclopeptides and Hg^{2+}, Pb^{2+} or Cd^{2+}, by isothermal titration microcalorimetry (ITC). Specific metal-ion signaling by the fluorogenic cyclopeptides was assessed by steady state fluorescence spectroscopy. The fluorescence emission spectral changes following the titration of the cyclopeptide with these metal ions were compared to evaluate changes upon peptide–metal-ion interactions. Standard Stern–Volmer formalism[27a] and the dependence of fluorescence intensity on quencher concentrations are presented. The results of these microcalorimetric and spectroscopic studies of complex formation between these cyclopeptides and heavy-metal ions show that fluorogenic cyclooctapeptides are structurally attractive for the rational design of chemosensors for heavy-metal ions.

2. Results and discussion

2.1. Isothermal calorimetric studies

Figure 2 shows a representative ITC curve of **CP2** and **CP3** with $Hg(ClO_4)_2$. As previously reported for **CP1**, these cyclopeptides also exhibit two-binding sites for Hg^{2+}.[19] The binding affinity values of these cyclopeptides and Hg^{2+} complexes are included in Table 1. The comparison of the binding affinity data of **CP1** and **CP2** for Hg^{2+} reveals that they exhibit similar binding constants for Hg^{2+} despite their primary structural differences in the locations of carboxylate groups, which are important metal-ion coordination sites. Although they demonstrate a similar binding affinity value for Hg^{2+}, the thermodynamic parameters associated with the formation of each complex type are distinctively different. For example, the first process associated with the formation of **CP1** and Hg^{2+} complex ($K_{a(1)} = 2.2 \times 10^6\ M^{-1}$) is both enthalpically and entropically favored. In contrast, **CP2** and Hg^{2+} complexation ($K_{a(1)} = 2.8 \times 10^6\ M^{-1}$) is enthalpically driven and entropically disfavored. The second binding enthalpy change for the **CP1** and Hg^{2+} interaction is positive. This equilibrium is driven by the increase in entropy associated with complexation ($K_{a(2)} = 6.5 \times 10^3\ M^{-1}$). On the other hand, the corresponding **CP2** and Hg^{2+} equilibrium is both enthalpically and entropically favored, driving the formation of the **CP2** and Hg^{2+} complex ($K_{a(2)} = 4.9 \times 10^4\ M^{-1}$).

Remarkably, **CP3** exhibited a thirty fold increase in binding affinity for Hg^{2+} ($K_{a(1)} = 7.9 \times 10^7\ M^{-1}$), compared to **CP1** and **CP2**, while retaining a strong affinity for Hg^{2+} at a second binding site ($K_{a(2)} = 1.7 \times 10^6\ M^{-1}$). These interactions are exothermic (Fig. 2b) and show a bis-cyclopeptide and Hg^{2+} complex formation,

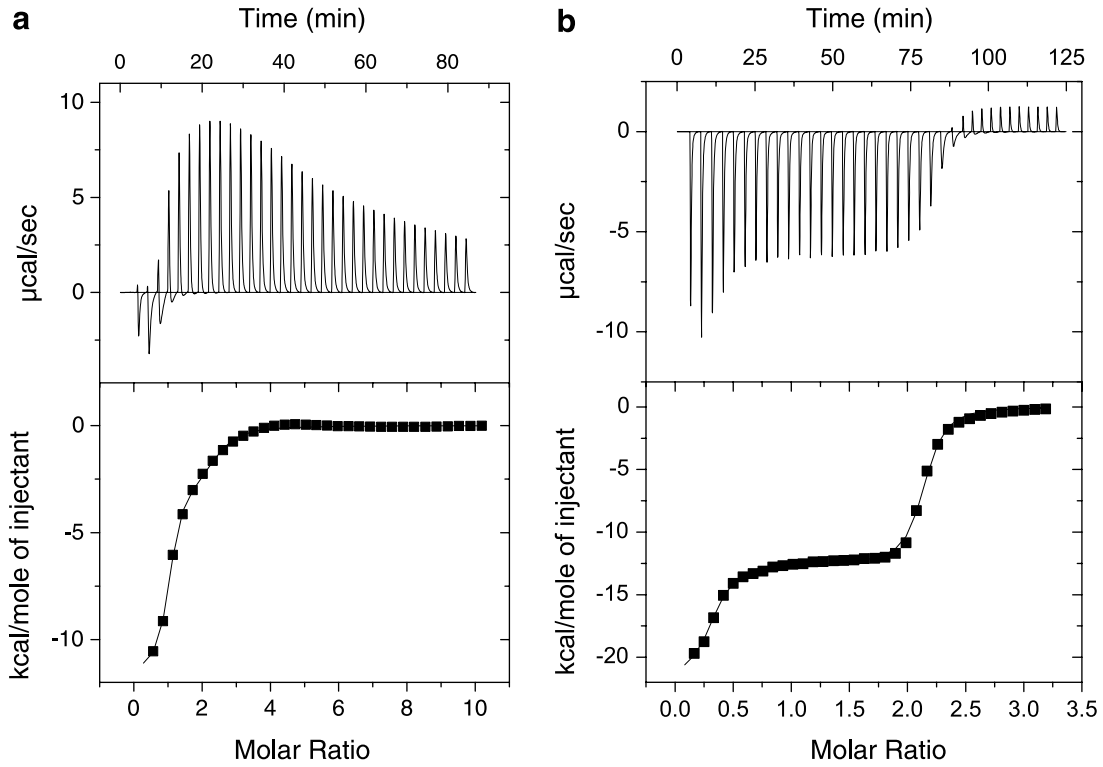

Figure 2. ITC data curve of **CP2** (a), and **CP3** (b), following titration with Hg^{2+}. Raw ITC titration data of 1.34 mL of **CP2** (0.14 mM) and **CP3** (0.15 mM) with 7 and 3 mM $Hg(ClO_4)_2$, respectively (top panels). Binding isotherms (bottom panels) are derived from the data in the corresponding top panels following correction for dilution and mixing effects.

Table 1. Thermodynamic parameters of metal-ion binding to cyclooctapeptides[a]

Metal ion[b]	Cyclopeptide	K_a (M^{-1})	ΔH (kJ mol^{-1})	ΔG (kJ mol^{-1})	ΔS (JK^{-1} mol^{-1})
Hg^{2+}[c]	**CP1**	$(2.2 \pm 1.0) \times 10^6$	-2.0 ± 0.8	-8.5 ± 1.0	21 ± 4
		$(6.5 \pm 1.7) \times 10^3$	6.5 ± 1.4	-5.2 ± 1.5	38 ± 4
	CP2	$(2.8 \pm 0.4) \times 10^6$	-11.2 ± 0.2	-8.9 ± 0.01	-7.8 ± 0.8
		$(4.9 \pm 0.8) \times 10^4$	-5.2 ± 1.2	-7.2 ± 0.6	6.5 ± 2.6
	CP3	$(7.85 \pm 0.4) \times 10^7$	-21.5 ± 0.1	-8.4 ± 0.8	-35.7 ± 2.9
		$(1.7 \pm 0.3) \times 10^6$	-12.2 ± 0.1	-6.6 ± 0.5	-12.4 ± 2.2
Pb^{2+}	**CP1**	$(2.0 \pm 0.5) \times 10^5$	1.4 ± 0.4	-7.3 ± 0.1	29 ± 1
	CP2	$(1.5 \pm 0.1) \times 10^5$	2.2 ± 0.4	-7.1 ± 0.01	31 ± 0.1
	CP3	—[d]	—	—	—
Cd^{2+}	**CP1**	$(1.3 \pm 0.2) \times 10^4$	6.6 ± 2.2	-5.7 ± 1.1	40 ± 7
	CP2	$(4.3 \pm 0.01) \times 10^4$	4.2 ± 0.5	-6.4 ± 0.01	35.3 ± 2
	CP3	—[e]	—	—	—

[a] Values correspond to the mean of three experiments and the standard error.
[b] Metal perchlorates.
[c] Hg^{2+} binds to two different binding sites, which exhibit different binding constants and thermodynamic parameters.
[d] Very small heat changes for this association prevented the calculation of the formation constants.
[e] No heat changes, which is indicative of the absence of bimolecular association.

suggesting an S–Hg^{2+}–S mode of coordination. In the presence of excess Hg^{2+}, a second **CP3** and Hg^{2+}-binding equilibrium is evident at a 1:2 **CP3**/Hg^{2+} stoichiometry. The binding isotherm for Hg^{2+} binding to **CP3** (Fig. 2b) shows sequential binding where Hg^{2+} binding at the second site is negligible in the equimolar range, but occurs in the presence of excess Hg^{2+}. Both these **CP3** and Hg^{2+}-binding equilibria are enthalpically driven (Table 1).

Figure 3 shows a representative ITC titration curve of **CP2** with $Pb(ClO_4)_2$ at 26 °C. The top panel shows the total measured heat associated with each titration of the Pb^{2+}, normalized by the molar ratio of Pb^{2+}/**CP2** in the calorimeter cell. The interaction is endothermic and shows a 2:1 stoichiometry with Pb^{2+}, suggesting a **CP**/Pb^{2+}/**CP** sandwich mode of complexation as previously reported for **CP1**.[19] This kind of sandwich complexation is consistent with the propensity of Pb^{2+} to form 1:2 complexes with ligands involving interligand π-stacking interactions.[22] Similar sandwich complexation has been reported by others for various types of macrocycle/metal-ion interactions,[17,18,21] and their preferences are attributed to the polarity and size of the macrocycle cavity and the charge, size, and coordination number of the metal ion(s) participating in the complex.

The calculated thermodynamic parameters of the interaction between **CP2** and Pb^{2+} are as shown in Table 1. These data are comparable to those obtained for the **CP1**/Pb^{2+}/**CP1** complexation, which is driven by the increase in entropy associated with this type of 2:1 stoichiometric complexation with Pb^{2+}. Although **CP3** shares a similar binding profile with Pb^{2+}, as demonstrated by **CP1** and **CP2**, its interaction with Pb^{2+} is weakly exothermic (Fig. 3b) and concurrently driven by an increase in entropy.

The binding isotherm profile for the interaction of **CP2** with Cd^{2+} is endothermic (Fig. 4a), therefore similar in its association with Pb^{2+}. As previously observed for **CP1**/Cd^{2+} complexation, this formation constant is about an order of a magnitude lower for Cd^{2+} ($K_a = 4.3 \times 10^4$ M^{-1}), compared to that for Pb^{2+} (1.5×10^5 M^{-1}). In contrast, **CP3** exhibited no significant bimolecular association with Cd^{2+}, as seen by the lack of heat changes following ITC measurements (Fig. 4b).

The above analysis of the interactions of **CP1** and **CP2** with Hg^{2+}, Pb^{2+}, and Cd^{2+}, shows that their binding affinities for each metal-ion type are similar, despite slight differences in the thermodynamic parameters associated with their underlying bimolecular interactions. These results show that changing the arrangement of the polar glutamyl residues in these cyclooctapeptides does not change their binding affinities for these metal ions. Although their associations with Hg^{2+} is generally exothermic, the positive enthalpy for the weaker second **CP1**/Hg^{2+} association (Table 1) could be attributed to the hydrophobic interactions between the amphipathic **CP1** macrocyles, which involve the non-polar side chain residues of Leu and Trp. In spite of this unfavorable enthalpy change, this second **CP1**/Hg^{2+} interaction is driven by the large entropy increase associated with this binding process. Conversely, the first **CP2**/Hg^{2+}-binding association is entropically disfavored and is driven by enthalpy (Table 1).

The binding of Pb^{2+} to **CP1** and to **CP2** is essentially similar within the experimental variations. These interactions are entropically driven albeit the associated unfavorable enthalpy changes, which may be attributed to the heats of dehydration of the hydrated cyclopeptide molecule and of the lead ion in aqueous solution following the formation of a stable **CP**/Pb^{2+}/**CP** complex. As previously noted, the peptides consist of polar groups that readily form hydrogen bonds with water molecules, whereas metal ions form ion–dipole interactions with dipolar water molecules. The latter interaction leads to the formation of hydration spheres around the metal ion. The positive ΔS values for the interaction between these cyclopeptides (**CP1** and **CP2**) and Pb^{2+} can be attributed to the reciprocal increase in the entropy of

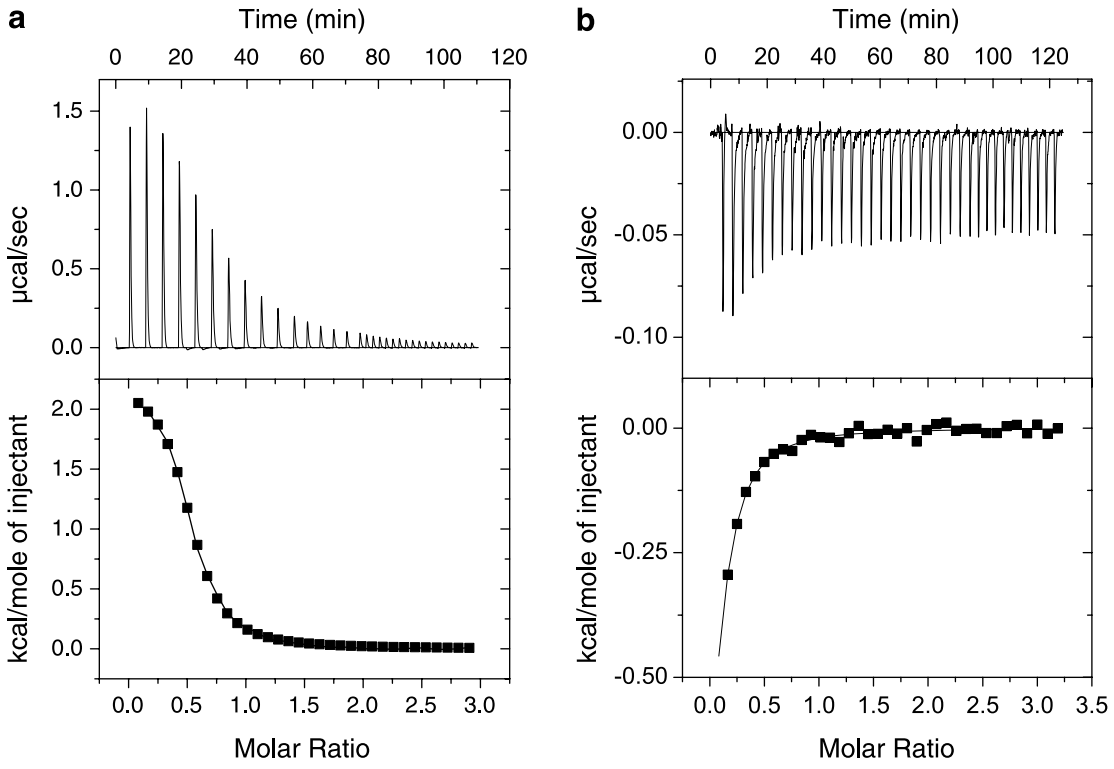

Figure 3. ITC data curve of **CP2** (a), and **CP3** (b), following titration with Pb^{2+}. Raw ITC titration data of 1.34 mL of **CP2** (0.14 mM) and **CP3** (0.15 mM) with 3 mM $Pb(ClO_4)_2$, (top panels). Binding isotherms (bottom panels) are derived from the data in the corresponding top panels following correction for dilution and mixing effects.

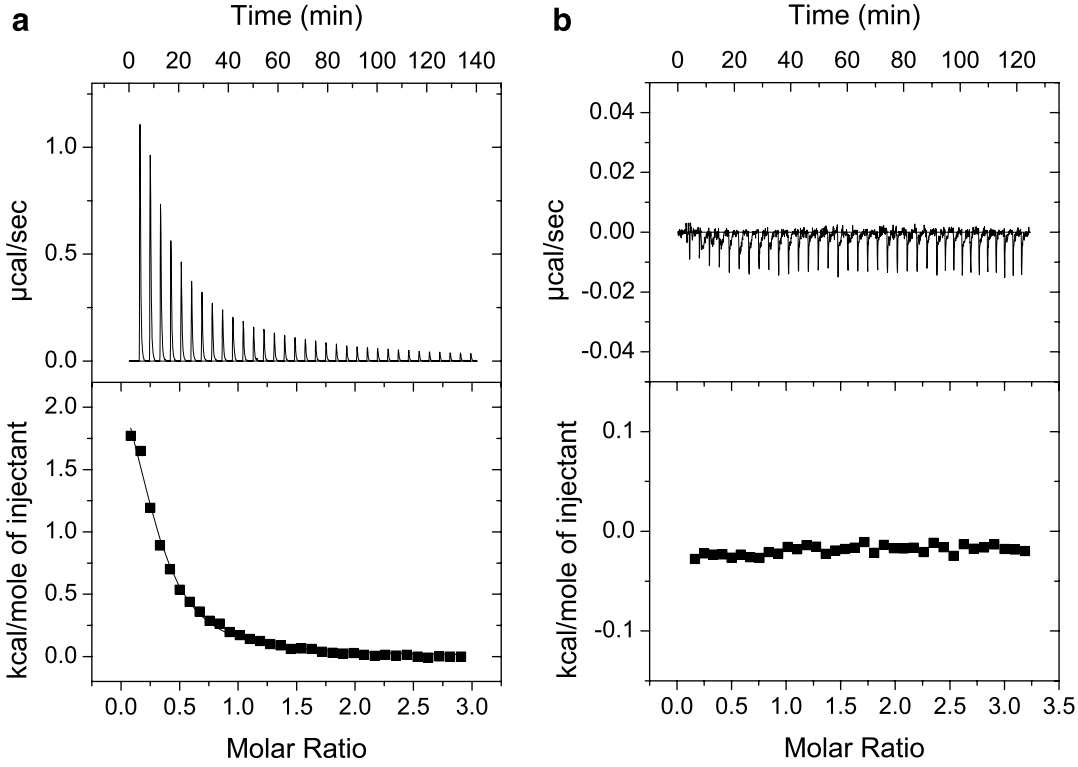

Figure 4. ITC data curve of **CP2** (a), and **CP3** (b), following titration with Cd^{2+} at 26 °C. Raw ITC titration data of 1.34 mL of **CP2** and **CP3** (0.15 mM) with 3 mM $Cd(ClO_4)_2$ at 33 injections of 6 µL each (top panels).

solvent molecules as a result of the above mentioned dehydration. Their corresponding associations with Cd^{2+} are similarly driven by this consequential increase in entropy due to dehydration, notwithstanding a reduction in their formation constant, which is approximately an order of a magnitude lower. The latter could be

ascribed to the smaller ionic radius of Cd^{2+} which lessens the stability of the **CP**/Cd^{2+}/**CP** complex (assuming a coordination number of 6, the ionic radii of Pb^{2+} and Cd^{2+} are 137 and 109 pm, respectively[28]).

As noted above, the interactions between the soft base donor containing cyclopeptide, **CP3**, and Hg^{2+} are significantly stronger than those exhibited by **CP1** and **CP2**. The enthalpy and entropy changes for the stepwise **CP3**/Hg^{2+} complex formation equilibria (Table 1) support an enthalpy favored association, as previously reported for simple cyclodextrin hosts and their molecular guests.[29] The stepwise **CP3**/Hg^{2+} associations correspond with **CP3**/Hg^{2+} ratios of 2:1 and 1:2 (Fig. 2b). The latter **CP3**(Hg^{2+})$_2$ species dominates at higher molar ratios of Hg^{2+}/**CP3**, as seen in the ITC-binding isotherm (Fig. 2b). Most sulfur bound mercury species commonly exhibit two- or four-coordinated complexes. The above bis-cyclopeptide and Hg^{2+} complex formation (**CP3**/Hg^{2+} 2:1) most likely involve two sulfur donor atoms in which the cysteinyl thiols from two molecules of CP3, sustain a linear S–Hg^{2+}–S complex. This S–Hg^{2+}–S mode of coordination effectively constitutes the high-binding association, which differentiates the **CP3**/Hg^{2+} associations from the **CP1**/Hg^{2+} and **CP2**/Hg^{2+} species. Corresponding, this S–Hg^{2+}–S coordination renders a second receptive binding site on the cyclopeptide involving the amide and carboxylate functionalities. Hence, with increasing amounts of Hg^{2+}, a second binding equilibrium takes place, which could be ascribed to the formation of the **CP3**(Hg^{2+})$_2$ species. Although the above explanation is in agreement with the tendency of Hg^{2+} to form linear complexes with 'soft base' donor atoms, it is speculative until they are successfully validated with structurally characterized (**CP3**)$_2$$Hg^{2+}$ and **CP3**(Hg^{2+})$_2$ data.

The binding isotherm for the interaction of Pb^{2+} with **CP3** is shown in Figure 3b. The heat change for this (**CP3**)$_2$$Pb^{2+}$ association is significantly smaller compared to the corresponding bimolecular interactions involving **CP1** and **CP2**. Since the heat of this association isotherm is too small to calculate the corresponding thermodynamic parameters with certainty, we could not obtain the formation constant for this bis-complexation. This phenomenon may indicate that the binding affinity of the **CP3**/Pb^{2+} complex is considerably weaker than that of the **CP1**/Pb^{2+} and **CP2**/Pb^{2+} systems. The two cysteinyl residues in **CP3** could weaken the formation of a stable **CP**/Pb^{2+}/**CP** sandwich complex and consequently diminish the heat of association. Remarkably, **CP3** showed no binding isotherm when titrated with Cd^{2+}, in contrast to **CP1** and **CP2** (Table 1), substantiating the impact of replacing two glutamyl with cysteinyl residues on the cyclooctapeptides.

2.2. Steady state fluorescence spectroscopy

The fluorescence spectra of **CP2** and **CP3** are characteristic of the emission spectrum of the indole group of tryptophan. These fluorophore-tagged cyclooctapeptides absorb near 280 nm and emit near 350 nm (Figs. 5a and 6a). Their emission shifts to longer wavelengths

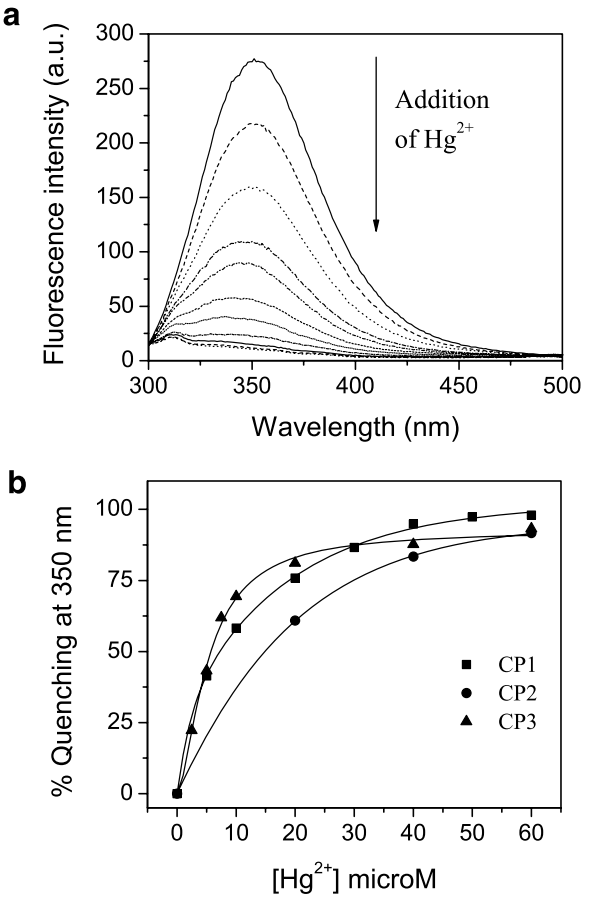

Figure 5. (a) Fluorescence emission spectrum of 10 μM **CP3** in the absence and presence of increasing concentrations of Hg^{2+} (2.5, 5, 7.5, 10, 20, 40, 60, 110 μM), and (b) Fluorescence quenching of 10 μM **CP1**–**3** (λ_{em} = 350 nm) in the presence of increasing concentrations of Hg^{2+}. Measured at 25 °C with λ_{ex} = 281 nm.

(red shift) relative to the emission of indole at 340 nm suggest that the indole group of these cyclooctapeptides are solvent exposed. They showed pronounced fluorescence quenching responses to Hg^{2+} and Pb^{2+}. This follows the general characteristics of diamagnetic 'heavy' ions such as Hg^{2+} and Pb^{2+}, which typically form complexes resulting in distinct fluorescence quenching. As previously observed for **CP1**,[19] the 'light' diamagnetic transition metal ion, Cd^{2+}, which generally forms fluorescent complexes, did not elicit any changes in **CP2** and **CP3** fluorescence. This may be ascribed to the weaker binding between these cyclopeptides and Cd^{2+} (Table 1).

Quenching of **CP2** fluorescence by increasing concentrations of Hg^{2+} follows a similar hyperbolic shape as shown by **CP1**, which is typical of the simple binding of a small molecule to its ligand (Fig. 5b).[19] The steepness of the hyperbolic curve increases for the corresponding quenching of **CP3** fluorescence by Hg^{2+}. This is indicative of larger fluorescence quenching of the indole fluorophore at lower concentrations of Hg^{2+}. Consequently, **CP3** signals the presence of Hg^{2+} more efficiently than **CP1** and **CP2**. Figure 6b shows quenching of **CP1**–**3** by increasing concentrations of

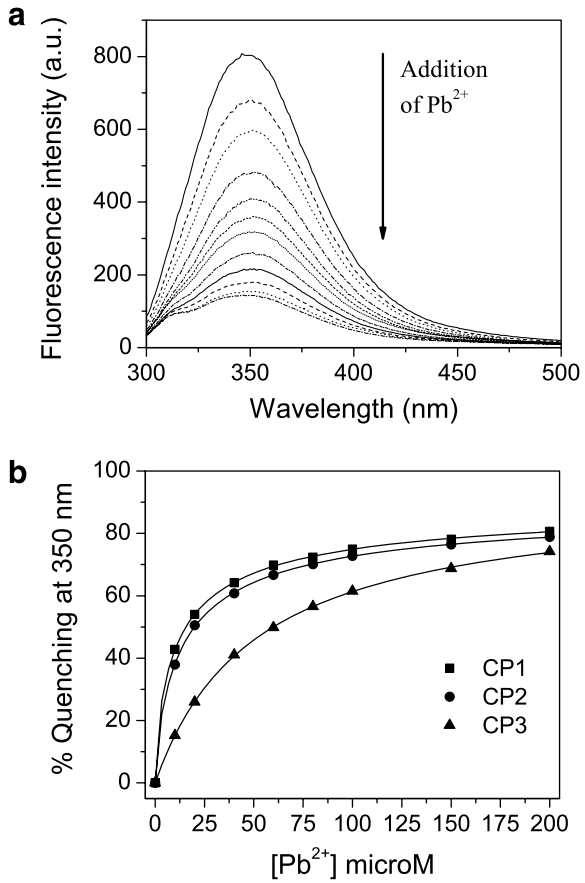

Figure 6. (a) Fluorescence emission spectrum of 10 μM **CP3** in the absence and presence of increasing concentrations of Pb^{2+} (10, 20, 30, 40, 50, 60, 80, 100, 150 μM), and (b) Fluorescence quenching of 10 μM **CP1**–**3** (λ_{em} = 350 nm) in the presence of increasing concentrations of Pb^{2+}. Measured at 25 °C with λ_{ex} = 281 nm.

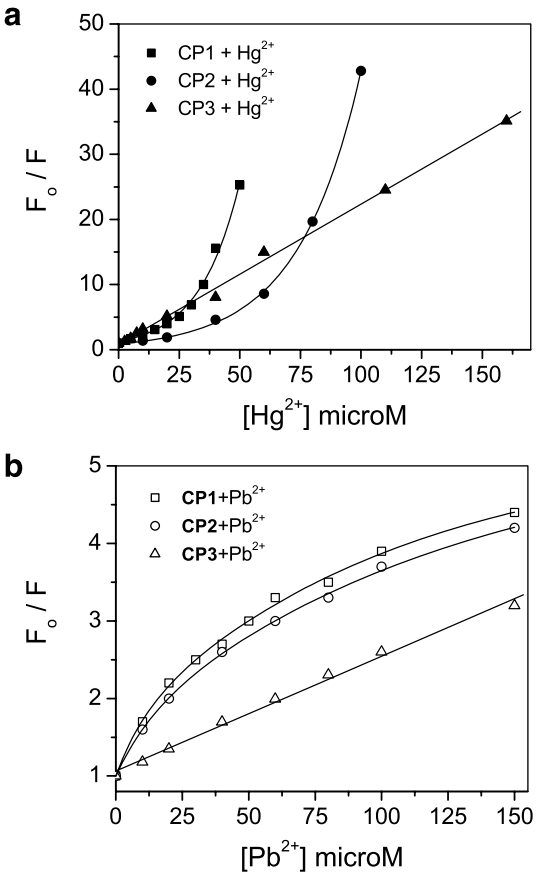

Figure 7. Stern–Volmer plot for Hg^{2+} (a), and Pb^{2+} (b) quenching of 10 μM **CP1**–**3**. (a) Exponential transformation of Hg^{2+} quenching of **CP1** and **CP2** yielded the least square regression lines, $y = 0.026x + 0.090$, and $y = 0.016x - 0.030$, respectively, with coefficients of determination, $r^2 > 0.99$. Line of best fit analysis of Hg^{2+} quenching of **CP3** yielded the linear regression line, $y = 0.2135x + 1$, where $r^2 > 0.99$. (b) Log transformation of Pb^{2+} quenching of **CP1** and **CP2** yielded the least square regression lines, $y = 2.31x - 0.81$, and $y = 2.20x - 0.79$, respectively, with coefficients of determination, $r^2 > 0.97$. Line of best fit analysis of Pb^{2+} quenching of **CP3** yielded the linear regression line, $y = 0.0155x + 1$, where $r^2 > 0.99$.

Pb^{2+}. **CP2** exhibited a similar fluorescence response to increasing concentrations of Pb^{2+} as shown by **CP1**. In contrast, the steepness of the slope decreases for the corresponding fluorescence response by **CP3**. Additionally, a limited <80% quenching by Pb^{2+} at saturating concentrations is measured for **CP1**–**3** as opposed to the >97% quenching at saturating concentrations of Hg^{2+}.

In order to understand the molecular interactions between these cyclopeptides and heavy-metal ions that result in fluorescence quenching, the data were analyzed using the Stern–Volmer formalism.[27a] Figure 7 shows the comparative Stern–Volmer plots for Hg^{2+} and Pb^{2+} quenching of **CP1**–**3**. The Stern–Volmer plots for **CP1** and **CP2** quenching by Hg^{2+} show an upward curvature, which is indicative of both complex formation (static quenching) and collisional (dynamic) quenching (Fig. 7a). Similar plots for quenching of these cyclopeptides by Pb^{2+} (Fig. 7b) show a downward curvature toward the *x*-axis. As previously reported for **CP1**, upon Pb^{2+}-binding **CP2** may adopt a conformation in which the fluorophore, Trp, is shielded from further quenching by these ions.[19] It is useful to note that the **CP**/Pb^{2+}/**CP** sandwich mode of complexation, as implicated from the ITC data (Section 2.1), could likely result in the shielding of the hydrophobic Trp flourophore by interligand interactions. This shielding effect could account for the limited 80% quenching by Pb^{2+} at saturating concentrations (Fig. 6b). The presence of these two indole fluorophore populations, in which one class is not accessible to the quencher, constitutes the deviation from linearity toward the *x*-axis in the Stern–Volmer plots.

Contrasting data were obtained for the quenching of **CP3** by Hg^{2+} and Pb^{2+}. In this case, Stern–Volmer intensities plots are linear (Fig. 7). This is indicative of a single class of fluorophore molecules in the sample that are equally accessible to the quencher. Therefore, F_o/F is linearly dependent upon the quencher concentration,[27a] and only one type of quenching occurs. Fluorescence quenching is described by the Stern–Volmer equation,

$$F_o/F = 1 + k_q\tau_o[Q] = 1 + K_{SV}[Q]$$

where F_o and F are the fluorescence intensities in the absence and presence of quencher, respectively; k_q is the bimolecular quenching constant; τ_o is the lifetime of the fluorophore in the absence of quencher, Q is the

concentration of the quencher, and K_{SV} is the Stern–Volmer constant, where $K_{SV} = k_q\tau_o$. The Stern–Volmer plot (Fig. 7a) shows a value of $K_{SV} = 2.14 \times 10^5\ M^{-1}$, which is too large to be due to collisional quenching. Assuming that an average unquenched lifetime of Trp is 3.1 ns,[27b] the value of the bimolecular quenching constant by Hg^{2+}, k_q, is $6.9 \times 10^{13}\ M^{-1}\ s^{-1}$, over a 1000-fold larger than the diffusion limited rate of $1.2 \times 10^{10}\ M^{-1}\ s^{-1}$.[27c] Hence, the fluorescence quenching of **CP3** by Hg^{2+} can be attributed to specific-binding associations as corroborated by the above described ITC data. Likewise, bimolecular quenching by Pb^{2+}, k_q is $5.0 \times 10^{12}\ M^{-1}\ s^{-1}$, can be ascribed to their binding associations (Fig. 7b). Fluorescence lifetime measurements, to be conducted in the near future, will conclusively determine the respective contributions of static and dynamic quenching and further our understanding of the underlying photochemical and photophysical processes.

3. Conclusion

The purpose of this work was to characterize the interactions of **CP1-3** with Hg^{2+}, Pb^{2+}, and Cd^{2+} in order to facilitate the design of cyclopeptides as sensors for heavy-metal ions. The ITC and fluorescence data revealed that complex formation is not significantly affected by the location of the carboxylate groups in the cyclooctapeptide. The underlying bimolecular formation constants between cyclooctapeptides **CP1** and **CP2** with Hg^{2+}, Pb^{2+}, or Cd^{2+} are similar. This result shows that changing the arrangement of glutamyl residues in these cyclooctapeptides does not change their binding affinities for these metal ions. However, the side chain thiolate functions have a significant impact on the complex formation process of **CP3**, resulting in an increase in both binding affinity and specificity for Hg^{2+}.

The macrocyclic octapeptide is an attractive structural scaffold which can be used as a framework for strategically positioning a great variety of donor atoms that are available from the repertoire of side chains from various types of amino acids. The results from this study show a significant difference in the Hg^{2+} binding ability and specificity upon the replacement of two Glu residues with two Cys residues in the cyclooctapeptide framework. In effect, the oxygen donor atoms ('hard bases') of Glu are replaced by the sulfur donor atoms ('soft bases') of Cys. Consequently, cyclooctapeptide **CP3** exhibit significantly improved molecular recognition for Hg^{2+} as previously reported for sulfur-containing calixarenes.[25,26] Accordingly, superior binding affinity and specificity for the toxic Hg^{2+} could be expected from replacing all of the four Glu residues of **CP2** with Cys residues. The replacement of donor atoms in the coordinating side chains with other coordinating groups such as the imidazole functionality of His, guanidinium group of Arg, phenolate of Tyr, sulfonic acid of cysteic acid, or phosphonic acids of phosphonotyrosine should contribute to a better understanding of the coordination geometry of cyclooctapeptide–metal-ion complexes, and accordingly, the design of better cyclopeptide complexing macrocycles with high metal ion selectivity. Understanding the coordination geometry of these complexes will also facilitate the design and positioning of the fluorophore in the cyclopeptide structural framework for maximal signal transduction, an essential feature of an effective chemosensor. In this study, the indole group of Trp, a naturally occurring amino acid, was conveniently employed as the sensing signal. Although the fluorescence spectral properties of Trp is well documented,[27b] it will not serve as an ideal reporting fluorophore for Hg^{2+} because its fluorescence is quenched in the presence of this heavy-metal ion. In future studies, we propose to substitute Trp with other fluorophores, which have been shown to exhibit fluorescence turn-on properties[30] in the presence of Hg^{2+}, such as derivatives of fluorescein,[6] mercaptopurine,[31] anthracene,[32] and 8-hydroxyquinoline[33] that could be covalently attached to the cyclooctapeptide scaffold via the ε-amino group of a Lys residue.

In this study, the interactions of cyclooctapeptides **CP1–3** with Hg^{2+}, Pb^{2+}, and Cd^{2+} were conducted by ITC. The range of binding constants which can be directly measured with ITC is between 10^2 and $\sim 10^9\ M^{-1}$. Hence, it is noteworthy that in evaluating cyclopeptides that exhibit tighter binding affinities for metal ions ($K_a > 10^9\ M^{-1}$), their binding constants could be measured by displacement isothermal titration calorimetry as reported by Sigurskjold.[34] This method was effectively used for analyzing the binding energetics of HIV-1 protease inhibitors.[35]

In summary, this paper describes the metal-ion binding preferences of **CP1–3**, their associated thermodynamic parameters, and the modulation of their fluorescence by Hg^{2+}, Pb^{2+}, and Cd^{2+}. The observed interactions and the related photophysical/photochemical responses will be useful for the rational design of cyclopeptides with strategic metalophilic coordination sites and intrinsic fluorophores that will show complexation-induced signals for sensing Hg^{2+}.

4. Experimental

4.1. Materials and methods

All chemicals were obtained from commercial suppliers and used without further purification. Fmoc-Glu(α-*O*-Allyl)-PAL-PEG-PS resin, Fmoc-L- and D-amino acids, and peptide coupling reagents were purchased from Novagen, EMD Chemicals Inc., CA. Reversed-phase HPLC columns (Vydac 214TP54 and 214TP510, 300 Å, 5 μm) were purchased from Chrom Tech, Inc. CP3 was obtained from SynBioSci Corporation, CA. All other chemicals were purchased from Aldrich Chemical Company.

4.2. Preparation of CP1 and CP2

CP2 was prepared by solid phase peptide synthesis by using the orthogonal protecting group strategy.[36] Fmoc-Glu(α-*O*-Allyl)-PAL-PEG-PS resin (1.25 g,

0.2 mmol) was loaded onto a column on the automated peptide synthesizer (Pioneer Peptide Synthesizer) and the linear synthesis was conducted as previously reported.[19] The crude peptide was purified by HPLC on a reversed phase C-4 or C-18 column to give the peptide as a white fluffy product following lyophilization. The mobile phase was 0.025 M triethylammonium acetate (A), and CH_3CN (B), delivered by the Rainin Dynamax 300 HPLC systems with UV monitoring at 214 nm. Conditions were 5% B to 30% B over 45 min with a flow rate of 5 mL/min. RP-HPLC for **CP1** (t_r = 32 min) and **CP2** (t_r = 27 min). The purified peptides were characterized by matrix-assisted laser desorption and ionization mass spectrometry (Applied Biosystems MALDI-TOF-MS) at the Mass Spectrometry Facility, Louisiana State University. MALDI-MS of **CP1** gave $[M+H]^+$/1044 (calculated 1043), $[M+Na]^+$/1066 (calculated 1065) and $[M+K]^+$/1082 (calculated 1082), and **CP2** $[M+H]^+$/1041 (calculated 1043), and $[M+2Na]^+$/1085 (calculated 1087).

4.3. Isothermal titration calorimetry

Microcalorimetric titrations of peptides with metal ions were conducted by isothermal titration microcalorimetry (ITC) using a Microcal VP-ITC Instrument. Experiments were carried out at 30 °C in water for **CP1** and **CP2** (pH 7), and in 10% acetonitrile at 26 °C for **CP3**. The peptide concentration ranged from 0.13 to 0.15 mM (1.34 mL sample cell), while the metal-ion concentrations varied from 3 to 10 mM in the syringe. Automated titrations were conducted until saturation, up to a ligand/peptide mole ratio of about 3 to 9. Heats of dilution and mixing for each experiment were measured by titrating the metal-ion solution into water or 10% acetonitrile. The effective heat of each peptide–metal-ion interaction was corrected for dilution and mixing effects. These heats of bimolecular interactions were obtained by integrating the peak following each injection of metal ion. The measurement of this heat change associated with each binding isotherm, a curve that represents the degree of saturation in terms of metal-ion to peptide mole ratio, allows an estimation of binding constants (K_B), reaction stoichiometry (n), enthalpy (ΔH) and entropy (ΔS), thereby providing a complete thermodynamic profile of the molecular interaction. The ITC data were analyzed by ITC Nonlinear Curve Fitting Functions for one or two-binding sites using the Microcal Origin 7.0 software (Microcal Sofware, Inc.). The line of best fit is the calculated curve using the best-fit parameters and it is used to determine the molar enthalpy change for binding, ΔH^o, and the corresponding binding constant, K_a.[37] The molar free energy of binding, ΔG^o, and the molar entropy change, ΔS^o, were derived from the fundamental equations of thermodynamics, $\Delta G^o = -RT \ln K_a = \Delta H^o - T(\Delta S^o)$.

4.4. Steady state fluorescence spectroscopy

Fluorescence spectroscopy measurements were carried out on a CARY Eclipse Spectrofluorometer, equipped with a thermostated cell holder. The fluorescence spectra were recorded using 1×10^{-5} M peptide solutions in a 1 cm quartz cell, which was maintained at 25 °C. The excitation wavelength was 281 nm and fluorescence emission at 350 nm was used in quenching studies. The dependence of fluorescence intensity on quencher concentrations was analyzed by the Stern–Volmer equation: $F_o/F = 1+K_{SV}[Q]$, where F_o and F are the fluorescence intensities in the absence and presence of the quencher, K_{SV} is the Stern–Volmer constant, and $[Q]$ is the concentration of the quencher.[27a]

Acknowledgments

The National Science Foundation, Grant #CHE 613675, supported this work. We also thank Martha Juban of Louisiana State University for assistance with the solid phase peptide synthesis of the cyclooctapeptides. W.G. and K.A. acknowledge the support from the NSF HBCU-Undergraduate Program at Winston-Salem State University.

References and notes

1. Czarnik, A. W. In *Chemosensors for Ion and Molecular Recognition*, Czarnik, A. W., Ed.; ACS Symposium Series 538; ACS: Washinghton, DC, 1993; Chap. 1 and references therein.
2. Tolosa, L.; Nowaczyk, K.; Lakowicz, J. In *Introduction to Laser Spectroscopy*; Andrews, D. L., Demidov, A. A., Eds., 2nd ed.; Kluwer: Kluwer Academic/Plenum, 2002; pp 139–170.
3. Ghosh, P.; Bharadwaj, P. K.; Mandal, S.; Ghosh, S. *J. Am. Chem. Soc.* **1996**, *118*, 1553.
4. White, B. R.; Liljestrand, H. M.; Holcombe, J. A. *Analyst* **2008**, *133*, 65–70.
5. Talanova, V. S.; Ropera, E. D.; Buiea, N. M.; Galina, G. *Tetrahedron Lett.* **2007**, *48*(45), 8022.
6. Nolan, E. M.; Racine, M. E.; Lippard, S. J. *Inorg. Chem.* **2006**, *45*(6), 2742, and references therein.
7. Aragoni, M. C.; Archa, M.; Demartin, F.; Devillanova, F. A.; Isaia, F.; Garau, A.; Lippolis, V.; Jalali, F.; Papke, U.; Shamsipur, M.; Tei, L.; Yari, A.; Verani, G. *Inorg. Chem.* **2002**(25), 6623.
8. Hayashita, T.; Qing, D.; Minagawa, M.; Lee, J. C.; Ku, C. H.; Teramae, N. . *Chem. Commun.* **2003**, *17*, 2160.
9. Zhang, X.-B.; Guo, C.-C.; Li, Z.-Z.; Shen, G.-L.; Yu, R.-Q. *Anal. Chem.* **2002**, *74*(4), 821.
10. Hu, X.; Pan, Z.; Wang, L.; Shi, X. *Spectrochim. Acta, Part A* **2003**, *59*, 2419.
11. Pedersen, C. J. *J. Am. Chem. Soc.* **1967**, *89*, 7017–7036.
12. Izatt, R. M.; Pawlak, K.; Bradshaw, J. S.; Bruening, R. L. *Chem. Rev.* **1991**, *91*, 1721.
13. Yordanov, A. T.; Whittlesey, B. R.; Roundhill, D. M. *Inorg. Chem.* **1998**, *37*, 3526.
14. Kraatz, H.-B. *Angew. Chem., Int. Ed. Engl.* **1994**, *33*, 2055.
15. Jang, Y. H.; Blanco, M.; Goddard, W. A., III *J. Am. Chem. Soc.* **1999**, *121*, 6142.
16. Bradshaw, J. S.; Krakowiak, K. E.; Tarbet, B. J.; Bruening, R. L.; Biernat, J. F.; Bochenska, M.; Izatt, R. M.; Christensen, J. J. *Pure Appl. Chem.* **1989**, *61*, 1619.
17. Heitz, F.; Kaddari, F.; Van Mau, N.; Verducci, J.; Seheno, H. R.; Lazaro, R. *Biochemie* **1989**, *71*, 71.
18. Chen, Y.; Han, K.-Y.; Liu, Y. *Bioorg. Med. Chem.* **2007**, *15*, 4537.
19. Ngu-Schwemlein, M.; Butko, P.; Cook, B.; Whigham, T. *J. Peptide Res.* **2006**, *66*(s1), 72.

20. Gates, W. D.; Rostas, J.; Kakati, B.; Ngu-Schwemlein, M. *J. Mol. Struct.* **2005**, *733*(1-3), 5.
21. Izzatt, R. M.; Pawlak, K.; Bradshaw, J. S.; Bruening, R. L. *Chem. Rev.* **1991**, *91*, 1721.
22. Hancock, R. D.; Martell, A. E. *Chem. Rev.* **1989**, *89*, 1875.
23. Sóvágó, I.; Ösz, K. *Dalton Trans.* **2006**, 3841.
24. Pearson, R. G. *Chem. Br.* **1967**, *3*, 103.
25. Delaigue, X.; Hosseini, M. W. *J. Chem. Soc., Chem. Commun.* **1995**, 609.
26. Gibbs, C. G.; Gutsche, C. D. *J. Am. Chem. Soc.* **1993**, *115*, 5338.
27. (a) *Principles of Fluorescence Spectroscopy*; Lakowicz, J. R., Ed., 3rd ed.; Springer Science and Business Media, LLC: New York, 2006; pp 277–305; (b) *Principles of Fluorescence Spectroscopy*; Lakowicz, J. R., Ed., 3rd ed.; Springer Science and Business Media, LLC: New York, 2006; p 64; (c) *Principles of Fluorescence Spectroscopy*; Lakowicz, J. R., Ed., 3rd ed.; Springer Science and Business Media, LLC: New York, 2006; p 282.
28. *Inorganic Chemistry – Principles of Structure and Reactivity*; Huheey, J. E., Keiter, E. A., Keiter, R. L., Eds., 4th ed.; Harper Collins: New York, 1993; pp 114–118.
29. Lofsson, T. J. *Pharm. Sci.* **1996**, *85*, 1017.
30. Rurack, K. *Spectrochim. Acta, Part A* **2001**, *57*, 2126.
31. Riva, B. S. V.; Costa-Fernandez, J. M.; Pereiro, R.; Sanz-Medel, A. *Anal. Chim. Acta* **2000**, *419*, 33.
32. Yoon, J.; Ohler, N. E.; Vance, D. H.; Aumiller, W. D.; Czarnik, A. W. *Tetrahedron Lett.* **1997**, *38*, 3845.
33. Prodi, L.; Bargossi, C.; Montalti, M.; Zaccheroni, N.; Su, N.; Bradshaw, J. S.; Izatt, R. M.; Savage, P. B. *J. Am. Chem. Soc.* **2000**, *122*, 6769.
34. Sigurskjold, B. W. *Anal. Biochem.* **2000**, *277*, 260.
35. Velazquez-Campoy, A.; Kiso, Y.; Freire, E. *Arch. Biochem. Biophys.* **2001**, *390*, 169.
36. Kates, S. A.; Daniels, S. B.; Albericio, F. *Anal. Biochem.* **1993**, *212*, 303.
37. Freire, E.; Mayorga, O. L.; Straume, M. *Anal. Chem.* **1990**, *62*, 950A.